Rashba splitting in *n*-type modulation-doped HgTe quantum wells with an inverted band structure

X. C. Zhang,* A. Pfeuffer-Jeschke, K. Ortner, V. Hock, H. Buhmann, C. R. Becker, and G. Landwehr
Physikalisches Institut der Universität Würzburg, Am Hubland, 97074 Würzburg, Germany
(Received 16 January 2001; published 29 May 2001)

Rashba spin splitting has been observed in the first conduction subband of *n*-type modulation-doped HgTe quantum wells (QW's) with an inverted band structure via an investigation of Shubnikov–de Haas oscillations in gated Hall bars. In accordance with calculations, no spin splitting was observed in the second conduction subband ($E2$), but an obvious Rashba splitting is present in the first heavy-hole-like conduction subband ($H1$) that displays a large dependence on gate voltage. Self-consistent Hartree calculations of the band structure based on an $8\times8\mathbf{k}\cdot\mathbf{p}$ model are compared with experiment, which enables us to understand and quantitatively describe the experimental results. It has been shown that the heavy-hole nature of the $H1$ conduction subband greatly influences the spatial distribution of electrons in the QW and also enhances the Rashba spin splitting at large electron densities. These are unique features of type III heterostructures in the inverted band regime. The $\beta k_{\|}^3$ dispersion predicted by an analytical model is a good approximation of the self-consistent Hartree calculations for small values of the in-plane wave-vector $k_{\|}$ and has consequently been employed to describe the spin splitting of the $H1$ conduction subband rather than the commonly used $\alpha k_{\|}$ dispersion for the conduction subband in type I heterojunctions. The relative magnitude of Rashba splitting in the $H1$ and $E2$ subbands as well as the splitting of the $H1$ subband for different well widths are also presented.

DOI: 10.1103/PhysRevB.63.2453XX PACS number(s): 73.21.Fg, 73.61.Ga, 71.70.Ej, 71.20.Nr

I. INTRODUCTION

Spin effects in semiconductor heterostructures have recently aroused much interest, not only from the fundamental point of view but also due to increasing interest in a transistor-like device that is based not on the electron charge, but on its spin.[1] It has long been known that the lack of inversion symmetry of the crystal lattice in bulk semiconductors can lift the spin degeneracy of electrons even in the absence of a magnetic field.[2] In structures with a reduced dimensionality, such as inversion layers or asymmetric quantum wells (QW's) with an asymmetrical confinement potential, lifting of the spin degeneracy at finite values of the in-plane wave vector is also expected, resulting in a finite spin splitting at the Fermi level in the absence of an external magnetic field. This splitting has historically been called Rashba spin splitting.[3,4] It was first observed in Shubnikov–de Haas (SdH) measurements for *p*-type GaAs/Al_xGa_{1-x}As heterojunctions by Störmer *et al.*[5] For narrow gap heterojunctions, it can be shown that the asymmetry of the macroscopic potential produces the dominant contribution to zero field spin splitting.[6,7] This splitting can be particularly large, for example, in *n*-type In_xGa_{1-x}As heterojunctions or QW's.[8–11] However even at the present, the Rashba effect still remains somewhat controversial. In the first theoretical investigation of a two dimensional system, Ohkawa and Uemura[12] concluded that, in a heterojunction with an asymmetric potential $V(z)$, the Rashba term is proportional to $\langle E\rangle=-1/e\langle\partial(E_c+V)/\partial z\rangle$, where E_c stands for the conduction band-edge profile and V for the space charge or applied electrostatic potential energy. However Därr, Kotthaus, and Ando[13] argued that the average value of the electric field $\langle E\rangle$ of the bound states in the first approximation is negligibly small. On the other hand, it has been pointed out by Lassnig,[14] and Winkler and Rössler[15] that this conclusion is not correct because the spin splitting of the conduction band is determined by the electric field in the valence band, $\langle E\rangle=-1/e\langle\partial(E_v+V)/\partial z\rangle$, based on a multiband Hamiltonian model, where E_v is the valence band-edge profile. Both de Andrada e Silva *et al.*,[16] and Pfeffer and Zawadzki[17] have shown that spin-dependent boundary conditions, as well as the penetration of the wave function into the barriers and its asymmetry at the interfaces, play an important role in Rashba spin splitting. This has been demonstrated in a recent experiment on In_xGa_{1-x}As QW's with both front and back gates.[18]

Compared to the relatively large number of previous experimental investigations of heterojunctions and QW's in III-V semiconductors,[8,11,10] narrow gap II-VI two-dimensional systems have been rarely investigated. Wollrab *et al.*[19] studied an inversion layer in *p*-type bulk $Hg_{1-x}Cd_xTe$. Rashba spin splitting in a gated, intrinsic HgTe/CdTe(112)B QW with a well width d_w of 11 nm was investigated by Schultz *et al.*[20] They calculated the Rashba parameter α and ascertained a linear dependence on carrier concentration based on a two-band model that presumes that spin splitting is linearly dependent on $k_{\|}$. Furthermore, they demonstrated that α can be as large as 4.5×10^{-9} eV·cm, which is almost three times larger than values reported for In_xGa_{1-x}As heterojunctions.[10] However, it will be demonstrated below that the first conduction subband for a HgTe QW with an inverted band structure, i.e., $d_w>6$ nm, has heavy-hole character and the spin splitting is proportional to $k_{\|}^3$ instead of $k_{\|}$.

Recently, magnetotransport studies of modulation doped $HgTe/Hg_{0.32}Cd_{0.68}Te(001)$ single quantum wells (SQW's) have been carried out.[21,22] The results can be readily explained by means of band-structure calculations based on the envelope function method. HgTe is a semimetal with a negative band gap of about 300 meV at low temperatures. It has a so-called inverted band structure, which means that the J_z

$=\pm 1/2$ branches of the Γ_8 band (which is called the light hole valence band in type I systems) act as conduction bands, and the Γ_6 and Γ_7 bands, and the $J_z=\pm 3/2$ branches of the Γ_8 band (the latter is called the heavy-hole band in type I systems) are valence bands. The light-hole conduction band and the heavy-hole valence band are degenerate at $k=0$ and the thermal energy gap is zero. When a HgTe layer is surrounded by $Hg_{1-x}Cd_xTe$ barriers with a gap on the order of 1 eV, electric subbands arise due to boundary quantization. For $HgTe/Hg_{0.32}Cd_{0.68}Te$ SQW's with a well thickness of less than 6 nm, the regular band sequence of a semiconductor occurs. However, for larger thicknesses, an inverted subband structure arises with energy spacings on the order of 10 meV, which means that the $E1$ subband falls below the $H1$ subband and becomes a valence subband, whereas the $H1$ subband becomes the first conduction subband.[23] The specific band alignment of HgTe QW's leads to a series of interesting phenomena, such as the formation of interface states.[24] In addition, Landau levels originating from the conduction subbands can cross those of the valence subbands.[25] The peculiar properties of the band structure of $HgTe/Hg_{0.32}Cd_{0.68}Te$ quantum well structures have been confirmed by magneto-optical experiments.[26]

In the following, we shall present magnetoresistance and Hall measurements on *n*-type modulation-doped QW's, whose band structures are in the inverted regime. The samples were symmetrically doped but it was possible to introduce an asymmetry in the QW potential by means of a top electric gate, i.e., the carrier concentrations could be changed substantially by applying a gate voltage. Fourier analysis of the SdH oscillations demonstrates the presence of Rashba spin splitting. The data are quantitatively explained via detailed self-consistent band calculations based on the envelope function method.

II. EXPERIMENTAL AND THEORETICAL DETAILS

HgTe SQW's were grown by molecular beam epitaxy on $Cd_{0.96}Zn_{0.04}Te(001)$ substrates at a temperature of 180 °C; growth details can be found in Ref. 21. The QW's were modulation doped symmetrically, on both sides of the HgTe QW in sample Q1605 with a well width of 21 nm, or asymmetrically, only on the substrate side of the HgTe QW in sample Q1651, with a well width of 12 nm, using CdI_2 as a doping material. The $Hg_{0.32}Cd_{0.68}Te$ barriers are composed of a 8-nm-thick spacer and a 9-nm-thick doped layer. A $Hg_{0.32}Cd_{0.68}Te$ cap layer of 5.5 nm thickness was subsequently grown, followed by an additional 40-nm-thick CdTe cap layer. The HgTe width was determined via a dynamic simulation of the (002) and (004) Bragg reflections.[27] The other thicknesses were estimated from the corresponding growth rates. After growth, a standard Hall bar was fabricated by means of a wet chemical etch, then a 200-nm-thick TiO_2 film, which serves as an insulating layer, was deposited by electron beam evaporation. Finally, Al was evaporated to form a gate electrode. Ohmic indium contacts were fabricated by thermal bonding. The samples were measured in a He^4 cryostat with standard lock-in techniques using a current of 1 μA at a temperature of 1.6 K and magnetic fields up to 14 T. The mobilities at zero gate voltage and 1.6 K are 1.3×10^5 and 3.5×10^5 $cm^2/(Vs)$ for the two specimens, with well widths of 12 and 21 nm, respectively.

TABLE I. Band structure parameters employed in the calculations for HgTe and CdTe at $T=0$ K in the $8\times 8\mathbf{k}\cdot\mathbf{p}$ Kane model.

	E_g (eV)	Δ (eV)	E_p (eV)	F	γ_1	γ_2	γ_3	κ	ϵ
HgTe	−0.303	1.08	18.8	0	4.1	0.5	1.3	−0.4	21
CdTe	1.606	0.91	18.8	−0.09	1.47	−0.28	0.03	−1.31	10.4

In order to interpret the experiments, self-consistent Hartree calculations based on an $8\times 8\mathbf{k}\cdot\mathbf{p}$ band-structure model including all second-order terms in the conduction and valence-band blocks of the 8×8 Hamiltonian have been carried out.[22,28] The inherent inversion asymmetry of HgTe and $Hg_{1-x}Cd_xTe$ has been neglected, because this effect has been shown to be very small in narrow gap systems.[6,7] The envelope function approximation was used to calculate the subbands of the QW's and the influence of the induced free carriers has been included in a self-consistent Hartree calculation. The valence-band offset between HgTe and CdTe was taken to be 570 meV based on recent experiments[27] and it was taken to vary linearly with barrier composition.[29] The band-structure parameters of HgTe and CdTe at 0 K employed in this investigation are listed in Table I and the energy gap of $Hg_{1-x}Cd_xTe$ is given by the empirical formula reported by Laurenti *et al.*[30]

III. RESULTS

As expected from its high electron mobility, the symmetrically modulation-doped sample Q1605 with a well width of 21 nm displays very pronounced SdH oscillations in magnetic fields between 0.7 and 14 T at a temperature of 1.6 K. In Fig. 1(a), the data up to 4 T have been plotted for various gate voltages, between −2.0 and 1.6 V. Fourier analysis of the complex SdH oscillations shows that at higher gate voltages three subbands are occupied. The results of the analysis are shown in Fig. 1(b). At a gate voltage V_g of 0.2 V, only two frequencies are resolved, which correspond to the $H1$ and $E2$ subbands, as will be explained below. No splitting of the $H1$ subband can be observed when the QW potential is symmetrical, i.e., $V_g\approx 0$ V. For either more positive or more negative gate voltages, a splitting of the $H1$ subband is apparent. Besides the main peaks labeled by $E2$, $H1+$, and $H1-$, there are other peaks at higher frequencies, which are due to the sums of the $E2$ and $H1$ peaks. The corresponding Hall resistance data in units of h/e^2 have been plotted in Fig. 2 as a function of the magnetic field B up to 14 T for various gate voltages, where h is Planck's constant and e is the electron charge. Well-developed quantum Hall plateaus can be seen, indicating the excellent quality of the sample. The largest Hall mobility was 6×10^5 cm^2/Vs at a gate voltage of 2.0 V; to our knowledge, this is the highest value that has been observed for HgTe QW's.

The results of self-consistent band-structure calculations for sample Q1605 are shown in Fig. 3. The energy of differ-

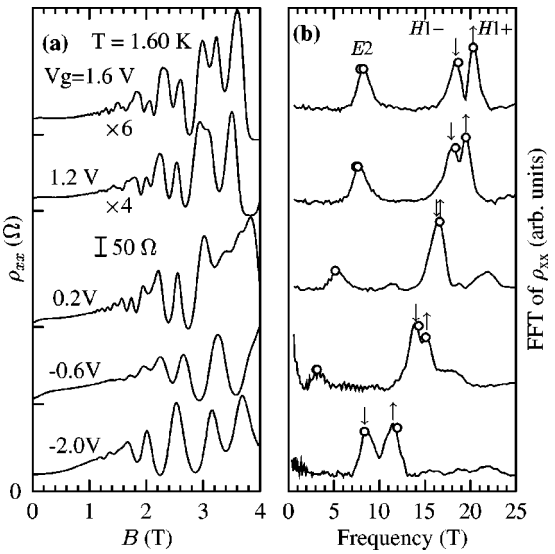

FIG. 1. SdH oscillations in $\rho_{xx}(B)$ (a) and the corresponding fast Fourier transformations (FFT) (b) for a *n*-type symmetrically modulation doped HgTe QW (Q1605) measured at 1.6 K and various gate voltages. In (a) the two uppermost curves have been multiplied by a factor of 6 and 4. In (b) the up and down arrows represent the two spin states of the $H1$ subband. The circles represent the results of theoretical calculations for the population of $H1$ and $E2$ subbands. It should be noted that these values were calculated using different depletion charge densities in the doped layer on the substrate side n_{ds} as discussed in the text. For $V_g > 0.2$ V, $n_{ds} = 0.55\ n_{sym}$; for $V_g < 0.2$ V, $n_{ds} = 0.45\ n_{sym}$; and for $V_g = 0.2$ V, $n_{ds} = 0.5\ n_{sym}$.

ent subbands has been plotted as a function of the in-plane wave-vector $k_\parallel$ for a symmetric and an asymmetric potential as dashed and solid lines, respectively. The corresponding gate voltages are 0.2 and -2.0 V, respectively. Using the

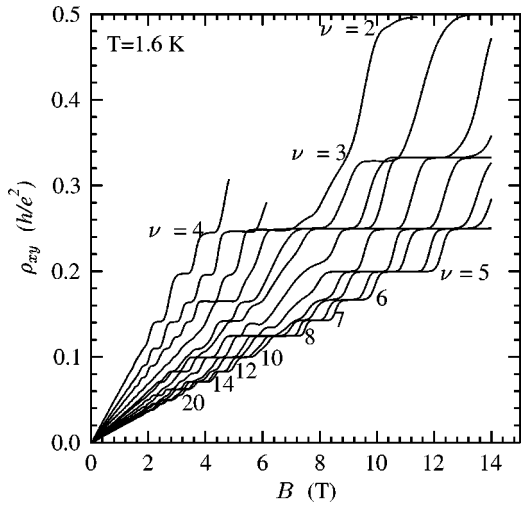

FIG. 2. Quantum Hall plateaus in $\rho_{xy}(B)$ for a *n*-type symmetrically modulation doped HgTe QW (Q1605) measured at 1.6 K and various gate voltages. From left to right, the curves correspond to the gate voltages of -2.4, -2.0, -1.6, -1.2, -0.8, -0.6, -0.2, 0.2, 0.6, 0.8, 1.2, and 1.6 V. The Landau level filling factors ν are also indicated.

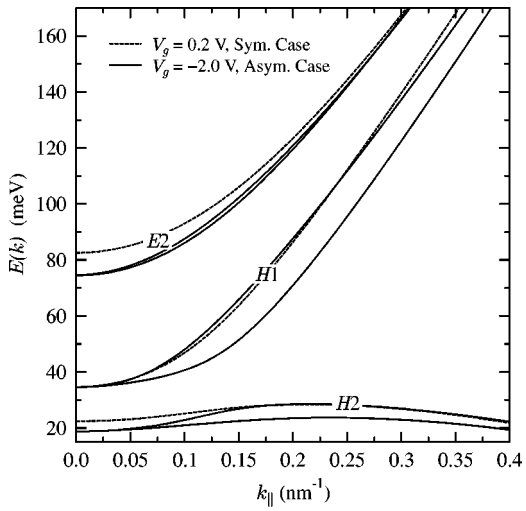

FIG. 3. The self-consistently calculated subband dispersion $E(k)$ of the HgTe QW Q1605 at two different gate voltages, $V_g = -2.0$ V (solid curve) and $V_g = 0.2$ V (dashed curve). The former represents the asymmetric case and the latter the symmetric case.

usual subband notation,[22] the conduction band has two branches, $H1$ and $E2$, and the valence band is the $H2$ subband. This is a consequence of the inverted band structure of QW's with a large well width in which the $E1$ subband is far below the $H1$ subband and is consequently not shown in Fig. 3. No splitting of the $H1$ and $E2$ subbands for the symmetric case is visible. However in the asymmetric case, a small spin splitting of the $E2$ subband at finite $k_\parallel$ is predicted, as well as a substantially larger splitting of the $H1$ subband. It should be mentioned here that the two spin split branches of the $H1$ subband cannot be designated as spin up and spin down because their eigenstates are not linearly polarized and do not carry a net magnetic moment.[31,32] The $H1$ and $E2$ subbands that are a mixture of states with different symmetries contain equal contribution of up and down spinor components at finite $k_\parallel$. The degeneracy of the $H2$ valence subband is also removed and one spin component has a larger maximum at finite $k_\parallel$, i.e., here we are dealing with an indirect band-gap semiconductor.

The corresponding band-edge potentials have been plotted for the symmetric and asymmetric cases in Fig. 4(a) and 4(b), respectively. Also shown are the electron probability distribution for both cases together with the Fermi energy E_F. The asymmetry of the charge distribution can clearly be seen as well as the penetration of the wave function into the barrier. Due to the heavy-hole character of the $H1$ subband, the maximum of the envelope function is shifted to the right side in Fig. 4(a), as will be discussed subsequently.

In Fig. 5, the total electron concentration versus gate voltage has been plotted as well as the carrier concentrations in the $E2$ subband and the spin split $H1+$ and $H1-$ subbands. The total electron concentration was determined from the Hall coefficient at low magnetic fields n_{Hall} and from the Fourier spectra of the SdH oscillations n_{SdH}. Both values agree very well over the entire gate voltage range. When the gate voltage is changed from -2.0 to 1.6 V, the electron density increases from 4.91×10^{11} to 1.33×10^{12} cm^{-2} with-

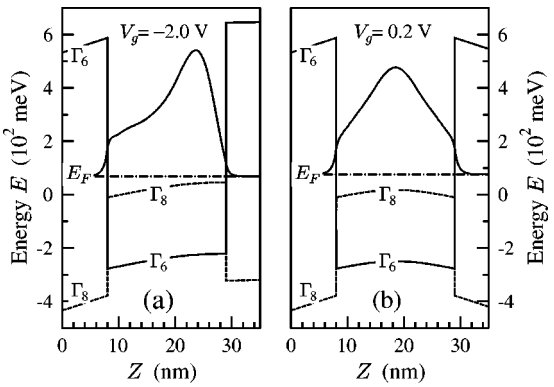

FIG. 4. The Γ_6 (solid) and Γ_8 (dashed) band-edge profiles and the electron probability of the $H1$ subband (thick solid curve) for $V_g=-2.0$ V in (a) and $V_g=0.2$ V in (b).

out any indication of a leakage current. $n_{SdH}=e/h(F_{1+}+F_{1-}+2F_2)$, where F_{1-} and F_{1+} are the corresponding frequencies of the $H1$ subband in Fig. 1(b) and F_2 that of the $E2$ subband. Winkler *et al.*[33] have argued that the above relations can only be applied when the anisotropic terms in the Hamiltonian can be neglected. This is the case here, the $E2$ and $H1$ subbands are nearly isotropic, as has been confirmed by our band-structure calculations. The slope of the n versus V_g plot changes abruptly at a gate voltage of -1.5 V. This is caused by the onset of the depopulation of the $E2$ subband. Because of the low electron concentration in this subband when V_g is between -1.0 and -1.5 V, no peaks could be reliably identified in the Fourier analysis and consequently no data points are shown for n_{E2} over this voltage range in Fig. 5. In order to estimate the total carrier concentration $n_{SdH}=n_{H1+}+n_{H1-}+n_{E2}$ between -1.0 and -1.5 V, the

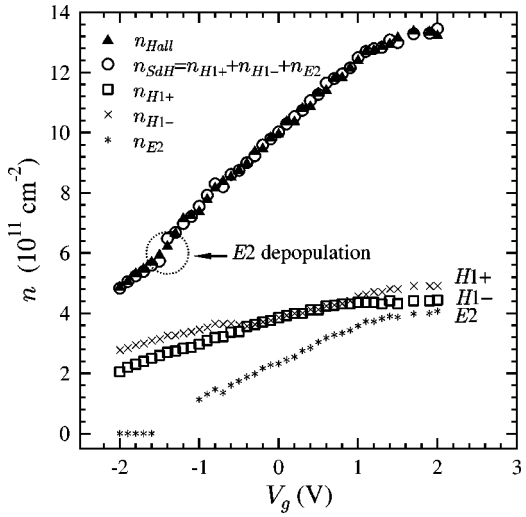

FIG. 5. Gate voltage dependence of carrier densities as deduced from the Hall coefficient, n_{Hall} (triangles), and from the Fourier transform spectra of the SdH oscillations, n_{SdH} (circles), for sample Q1605. The carrier densities for the $E2$ subband, n_{E2} (asterisks), and the two spin components of the $H1$ subband, n_{H1+} (squares) and n_{H1-} (crosses) are also shown. The dashed circle indicates the region in which the onset of depopulation of the $E2$ subband occurs.

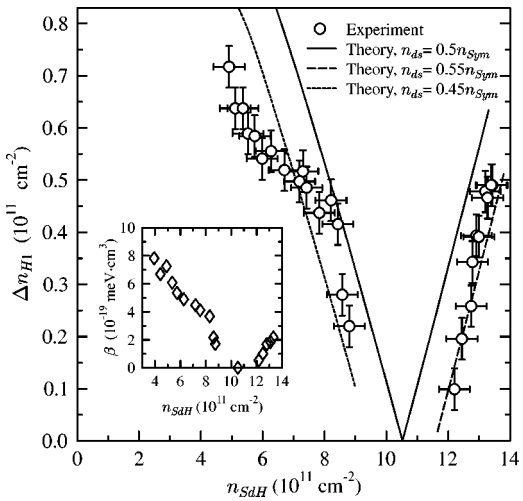

FIG. 6. Experimental (circles) and calculated (lines) population differences Δn_{H1} in the two spin states of the $H1$ subband as a function of the total charge-carrier density, n_{SdH}. The n_{ds} parameter is the depleted charge density in the doped layer on the substrate side. n_{sym} is the carrier density when the QW potential is symmetric. This corresponds to the point when $\Delta n_{H1}=0$. The theoretical results for different n_{ds} are shown as lines. The inset shows the spin-orbit interaction constant β at various carrier densities which are controlled by the gate voltage.

electron concentration n_{E2} for this range was obtained by extrapolation of the data points at higher gate voltages. It should be noted here that one is dealing with a multiple carrier system and the determination of the electron concentration from the Hall coefficient is not straightforward, nevertheless, the good agreement between the SdH and Hall data indicates that the approach chosen here is reasonable; it can be shown for a two carrier model,[34] that the Hall coefficient $R_H\approx 1/(n_1+n_2)$ if the mobilities of the two carriers are large enough, $\mu_1 B\gg 1$ and $\mu_2 B\gg 1$. Hence, R_H is indeed related to the total carrier concentration.

Using the calculated band structure, the carrier densities in the $H1+$, $H1-$, and $E2$ subbands have been calculated at various gate voltages. The results for selected gate voltages are shown in Fig. 1(b) as frequencies by empty circles and are in good agreement with the experimental data. The experimental population differences between the two spin states of the $H1$ subband for all gate voltages are shown in Fig. 6 as circles and the theoretical differences as lines.

IV. DISCUSSION

Our data clearly demonstrate that spin splitting is caused by an asymmetrical potential in single HgTe quantum wells. Our results and the subsequent analysis show that one can extract information about Rashba spin splitting from experiments at relatively high magnetic fields. Because only one $H1$ peak is resolved for the symmetric case, i.e., $V_g\approx 0.2$ V, Zeeman spin splitting can be excluded. This is corroborated by the fact that the peak frequencies in the Fourier spectra of the SdH oscillations remain the same irrespective of the maximum magnetic field B_{max} used in the transforma-

tion process, for example, $B_{max}=3$, 5, and 10 T yield the same result. Furthermore, experiments in tilted magnetic fields allow us to distinguish between Zeeman and Rashba splitting. In a two dimensional electron gas, Zeeman splitting depends on the total magnetic field. SdH experiments carried out in tilted magnetic fields have shown that the peaks in the Fourier transform spectra depend only on the normal component of the magnetic field, thus excluding Zeeman splitting. Previously, Rashba splitting has been demonstrated through the analysis of beating patterns in the SdH oscillations at relatively low magnetic fields, where the Zeeman spin splitting was unresolved. We do not expect a clear beating pattern in the SdH oscillations for the asymmetric case in the low-field range because of destructive interference effects due to the presence of three subbands. At gate voltages when only the two spin states of the $H1$ subband are occupied, beating effects are visible in the first derivative of the magnetoresistance with respect to B.

In Fig. 6, the experimental values and the theoretical calculations of the difference in population Δn_{H1} between the two spin states of the $H1$ subband are plotted versus the total carrier concentration n_{SdH}. Here, the total carrier density n_{SdH} has been employed rather than the carrier density in only the $H1$ subband n_{H1} because the electric field $\langle E \rangle$ is, to a good approximation, proportional to n_{SdH}. The calculated carrier densities in both the $H1$ and $E2$ subbands at various gate voltages agree with the experimental values for a well width d_w of 21 ± 2 nm. A simulation of the x-ray diffraction results gives a value of 22 ± 2 nm, in agreement with the above value. It should be emphasized that the occupation of the $E2$ subband depends mainly on the well width and not on the details of the self-consistently calculated Hartree potential. Furthermore, the well width, and hence, the calculated carrier densities for two additional QW's, an asymmetric and a symmetric QW have been corroborated by simulations of the corresponding x-ray diffraction results. The asymmetric sample had no gate, so that the carrier concentration is constant. The observed Rashba spin splitting for an electron concentration of 1.34×10^{12} cm^{-2} agrees very well with the band-structure calculations.[35]

For $n_{SdH}=1.05\times10^{12}$ cm^{-2}, i.e., $V_g=0.2$ V and $\Delta n_{H1}=0$, which corresponds to the symmetric case, the resulting band-edge profile and the electron probabilities are shown in Fig. 4(b). The gate voltage of $V_g\approx0.2$ V required to produce a symmetric QW structure was determined by comparing the experimental values of the carrier densities in the $H1$ and $E2$ subbands with theoretical calculations. This is obvious from the similar sizes of the experimental spin splitting in the $H1$ subband at gate voltages of 1.0 V and -0.5 V shown in Fig. 1(b). If V_g differs appreciably from this value, the symmetry of $V(z)$ decreases, see Fig. 4(a), which results in a nonzero spin splitting at finite $k_\parallel$.

A very distinctive feature of the distribution of the envelope function in the $H1$ subband should be noted here. As can be seen in Fig. 4(a), the maximum of the envelope function is not located near the minimum of the confinement potential for the asymmetrical case as is true in type I heterojunctions, but is shifted significantly to the opposite side of the QW. This is due to the fact that in a type III HgTe QW

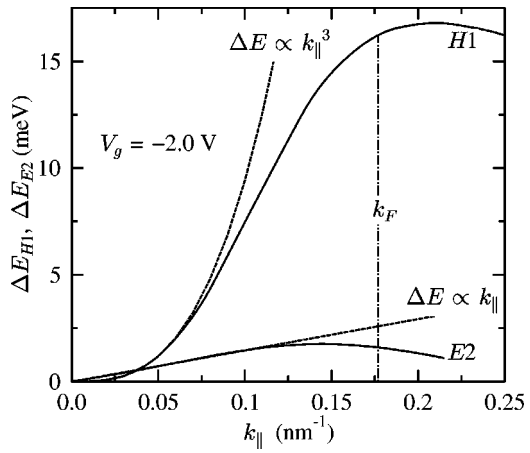

FIG. 7. The calculated spin splitting energy of the $H1$ and $E2$ subbands (solid curves), ΔE_{H1} and ΔE_{E2}, versus in-plane wave-vector $k_\parallel$ for sample Q1605 at $V_g=-2.0$ V. The position of the Fermi wave-vector k_F is denoted by the dotted-dashed line. The two dashed lines demonstrate that ΔE_{H1} and ΔE_{E2} are proportional to $k_\parallel^3$ and $k_\parallel$, respectively, at small $k_\parallel$.

with an inverted band structure, the $H1$ conduction band is principally a heavy-hole state as far as the Bloch components of the envelope function are concerned. At $k_\parallel=0$, the $H1$ subband is a pure heavy-hole state, namely $|\Gamma_8,\pm3/2\rangle$. Even for a wave vector at the Fermi surface, $k_F=0.25$ nm^{-1} (corresponding to a carrier density of 10^{12} cm^{-2}), 60% of the $H1$ subband states are $|\Gamma_8,\pm3/2\rangle$. The heavy-hole nature of the $H1$ conduction band shifts the peak position of $|\psi(z)|^2$ away from the higher doped side of the QW. This is an unique feature of type III inverted semiconducting QW's. Moreover the larger spin-orbit interaction in the heavy-hole subband also explains the large Rashba spin splitting in the $H1$ subband of about 17 meV at the Fermi wave vector as shown in Fig. 7 for $V_g=-2.0$ V.

The gate voltage has been introduced as a variable in the numerical simulation by employing the sheet carrier density inside the QW as an input parameter. We assume that the top gate voltage does not influence the status of the doped layer on the substrate side; this implies that the depleted charge density on the substrate side, denoted by n_{ds}, remains constant and is exactly one half of the carrier density n_{sym} over the entire gate voltage range. n_{sym} is the carrier density when the potential of the QW is symmetric, i.e., when $V_g=0.2$ V. Using this assumption, the theoretical results shown by the solid lines in Fig. 6 are slightly larger than the experimental values, however, if the uncertainties in both the experimental values and the material parameters employed in theoretical calculations are taken into consideration, the agreement between theory and experiment is reasonable. This is also true for the carrier densities in separate subbands, i.e., in the $E2$ subband and the spin-split states of the $H1$ subband, as shown by the empty circles in Fig. 1(b).

However, the depleted charge density on the substrate side n_{ds} is unknown and can therefore be regarded as an adjustable parameter. Obviously a slight change in the asymmetry of the confinement potential can significantly influence the Rashba spin splitting. For example, if we employ values

of $0.45n_{sym}$ and $0.55n_{sym}$ for the negative and positive gate voltage ranges, respectively, Δn_{H1} shows better agreement with experiment, as indicated by the dot-dashed and dashed curves in Fig. 6. It should be noted here that if n_{ds} is assumed to be smaller than $0.5n_{sym}$ for a negative gate voltage, then it is physically meaningful to assume that n_{ds} is larger for a positive voltage. When V_g is positive, the potential in the QW is lowered and additional electrons can come from the substrate side resulting in a n_{ds} larger than $0.5n_{sym}$, even though most of the electrons still originate from the top side; when V_g is negative, the converse is true, i.e., some electrons can escape from the QW to the doped barrier on the substrate side resulting in a n_{ds} smaller than $0.5n_{sym}$. This also reflects the fact that the electric field along the growth direction plays an important role in the spin splitting.[17,11] As pointed out by Pfeffer and Zawadzki[36] and Hu *et al.*,[11] a detailed distribution of the electric field in the QW is always unknown and it is not clear to what extent one can rely on the field distribution obtained by fitting the measured total electron concentration based on self-consistent subband-structure calculations, as has been done here. Nevertheless, it is obvious that our experimental results can be satisfactorily reproduced by means of multiband Hamiltonian calculations.

Spin splitting in the conduction subband of type I heterostructures has been described using a one-band model $E^{\pm}(k_{\|})=E_0+\hbar^2k_{\|}^2/2m^*\pm\alpha k_{\|}$ with the Rashba spin-orbit interaction constant α. Some authors have attempted to include nonparabolicity to some extent in their analysis by using a modified two-band model.[11,19,20] Both models result in a splitting with a linear dependence on $k_{\|}$. But it is well known that these models are not applicable for narrow-gap heterostructures. Self-consistent calculations[15,32] as well as analytical model calculations[16] for type I narrow gap systems have shown that the spin splitting is linear only for small $k_{\|}$ but tends to be constant for larger $k_{\|}$ due to band nonparabolicity effects. We have found similar spin splitting predictions from self-consistent calculations for asymmetric $HgTe/Hg_{0.32}Cd_{0.68}Te$ type III heterostructures with well widths less than 6 nm. These structures have a normal semiconducting band structure, in which the $E1$ subband is the first conduction subband. In this case, the spin splitting is linear for small $k_{\|}$ and approaches a constant value for larger $k_{\|}$. Furthermore, spin splitting in the first and second conduction subband is of the same order of magnitude, which depends very much on the details of the heterostructure. For HgTe QW's with larger well widths and consequently an inverted band structure, as is the case here, the situation is more complicated. Fig. 7 displays the spin splitting energies of the $H1$ and $E2$ subbands, ΔE_{H1} and ΔE_{E2}, as a function of $k_{\|}$ for the calculated band structure shown in Fig. 3, i.e., the asymmetric case for $V_g=-2.0$ V. The ΔE_{H1} versus $k_{\|}$ plot starts with a nearly zero slope at $k_{\|}=0$, increases nonlinearly, and then finally begins to decrease for increasing $k_{\|}$ due to band mixing, i.e., nonparabolicity effects. Spin splitting reaches a maximum value slightly above the Fermi wave vector. This is another unique feature of the inverted band structure and one more consequence of the heavy-hole character of the envelope function for the first conduction subband. ΔE_{H1} can be described very well at small values of $k_{\|}$ by a $k_{\|}^3$ dispersion,[32] as indicated by the upper dashed line in Fig. 7. On the other hand, the spin splitting of the $E2$ subband displays a linear behavior at small values of $k_{\|}$, as shown by the lower-dashed line in Fig. 7.

Consistent with the above discussion, Winkler[32] has shown that spin splitting should be proportional to $k_{\|}^3$ for the heavy-holelike state $|\Gamma_8,\pm 3/2\rangle$, but for the electronlike state $|\Gamma_6,\pm 1/2\rangle$ and the light-holelike state $|\Gamma_8,\pm 1/2\rangle$, spin splitting should be a linear function of $k_{\|}$. This is in good agreement with the self-consistently calculated ΔE_{H1} and ΔE_{E2} versus $k_{\|}$ behavior shown in Fig. 7; the $H1$ conduction subband in a type III HgTe QW with an inverted band structure is principally a heavy-hole state, and the $E2$ subband is an admixture of the light hole and electron state. As suggested in Ref. 32, the spin split heavy-hole subband dispersion can be expressed as

$$E_{\pm}(k_{\|})=\frac{\hbar^2k_{\|}^2}{2m^*}\pm\beta k_{\|}^3, \tag{1}$$

where β is the spin-orbit coupling constant[37] between the Γ_8 and Γ_6 bands. The $n_{H1\pm}$ densities in the spin split $H1$ subbands can be expressed by[32]

$$n_{H1\pm}=\frac{n_{H1}}{2}\pm\frac{\sqrt{2}m^*\beta n_{H1}}{\hbar^2X}\sqrt{\pi n_{H1}(6-4/X)}, \tag{2}$$

where

$$X=1+\sqrt{1-4\pi n_{H1}(2m^*\beta/\hbar^2)^2}. \tag{3}$$

From Eqs. (2) and (3) one can easily show that

$$\beta=\frac{\hbar^2}{2m^*}\sqrt{\frac{X(2-X)}{4\pi n_{H1}}}, \tag{4}$$

and

$$X=\frac{2(2+\sqrt{1-a^2})}{a^2+3}, \tag{5}$$

where $a=\Delta n_{H1}/n_{H1}$. Making use of Eqs. (4) and (5) results in the spin-orbit interaction parameter β, which is shown as a function of n_{SdH} in the inset of Fig. 6. Because of a lack of experimental values for the effective mass m^*, theoretical band edge values of m^* at various gate voltages have been employed, for example, a typical value at $V_g=0.2$ V is $0.034m_0$. Analogous to α for a linear dependence, β can only correctly describe the spin splitting at small values of $k_{\|}$. At larger values, for example, only a rough estimate of the spin splitting can be expected at the Fermi wave vector for a given gate voltage and obviously β cannot describe the spin splitting for all $k_{\|}$.

A few comments on the relative magnitude of the spin splitting in $E2$ and $H1$ subbands are appropriate. De An-

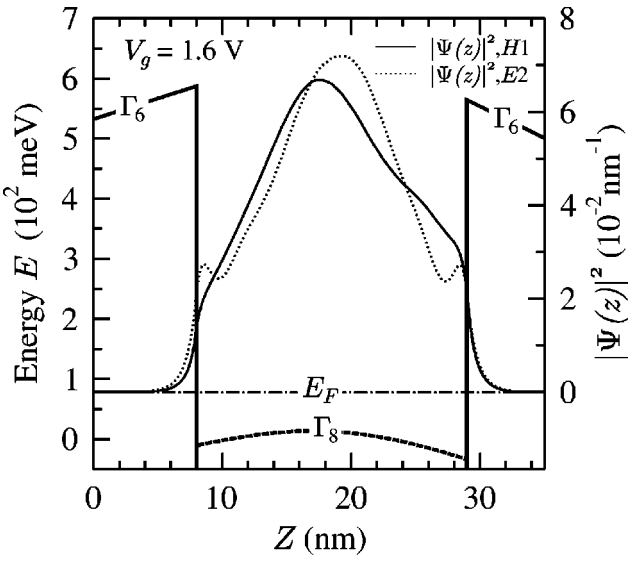

FIG. 8. Γ_6 (thick solid line) and Γ_8 (thick dashed line) band-edge profiles and the spatial electron density probabilities for the $H1$ subband (thin solid line) and the $E2$ subband (thin dotted line), at $V_g = 1.6$ V for sample Q1605.

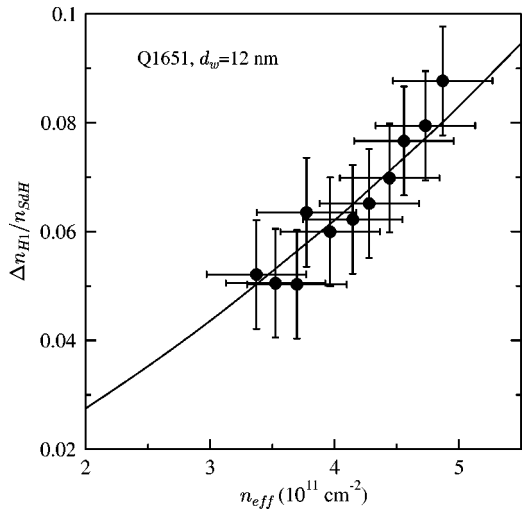

FIG. 9. Experimental values of the relative population difference between the two spin states of the $H1$ subband $\Delta n_{H1}/n_{SdH}$ versus the effective carrier density $n_{eff}=n_s-n_{sym}$ for a 12 ± 2 nm (Q1651, filled circles) thick QW. The corresponding theoretical calculations for a well width of 13 nm (solid line) is also shown. In these calculations, $n_{ds}=0.5n_{sym}$ has been used.

drada e Silva *et al.*[16] as well as others[10,17] have shown that the main contribution to the spin splitting is not due to the mean electric field but due to the asymmetry of the envelope function at the interfaces. Their theories are not directly applicable for type III heterostructures with an inverted band structure because of the significant influence of the heavy-hole states. Nevertheless, due to the lack of an analytical model for type III heterostructures, we shall qualitatively discuss our numerical results in terms of these theories in the following. By means of self-consistent calculations utilizing Schrödinger's and Poisson's equations, we have calculated the density distribution $|\psi(z)|^2$ for both the $E2$ and $H1$ subbands. Figure 8 depicts the resulting band-edge profile and the normalized electron probability along the z direction for both subbands. The electron probability for the $H1$ subband has a more asymmetric distribution along the z direction, as can be obviously seen near the two interfaces of the QW. The maximum of the electron probability of the $H1$ subband is shifted away from the minimum of the confinement potential rather than towards it as is the case for type I heterojunctions. This is once again a consequence of the heavy-hole nature of the $H1$ subband in type III QW's with an inverted band structure, as discussed above. We have also calculated the expectation value of the electric field weighted by the electron probability densities $\langle E\rangle=\int dz[d\phi(z)/dz]\cdot|\Psi^2(z)|$ for both subbands according to Ref. 10, where $\phi(z)$ is the Hartree potential. The expectation value of the electric field is 11% larger in the $H1$ than in the $E2$ subband. This small difference cannot be the reason for the much smaller spin splitting in the $E2$ subband compared to the $H1$ subband predicted by the numerical calculations. Therefore, the main contribution to spin splitting is apparently due to the asymmetry of the electron probability density at both interfaces as is also the case for type I heterostructures. But in contrast to type I structures, where spin splitting in the first and second subband is comparable,[11,15,16] spin splitting in the $E2$ subband has not been observed in this investigation over the entire range of gate voltages. Furthermore, theoretical calculations predict a much smaller splitting for the $E2$ subband compared to the $H1$ subband. Hence, the heavy-hole nature of the $H1$ subband increases the spin splitting compared to the $E2$ subband as a consequence of the asymmetry of the envelope functions. This unique feature of type III heterostructures with an inverted band structure is corroborated by the excellent agreement between the experimental and numerical results.

In Fig. 9, experimental values and theoretical calculations of the relative population difference between the two spin states of the $H1$ subband are plotted versus the effective carrier density n_{eff} for a 12-nm-wide asymmetrically doped QW. $n_{eff}=n_{SdH}-n_{sym}$ is defined as the effective net charge density and roughly describes the degree of potential asymmetry of the QW. The electron concentration n_{sym} for this sample is 1.16×10^{12} cm^{-2}. In this specimen E_{H1}, E_{E2} and E_{E2-H1} are larger in comparison with the 21 nm sample and only the first conduction subband $H1$ is occupied. It can be seen that the theoretical calculations are in good agreement with the experimental results.

V. CONCLUSIONS

In conclusion, we have investigated Rashba spin splitting in HgTe SQW's with an inverted band structure by means of gate controlled Hall devices. Spin splitting of the $H1$ subband shows a large gate voltage dependence. In contrast, spin splitting of the $E2$ subband is experimentally unresolved. Band structure calculations based on the $8\times8\mathbf{k}\cdot\mathbf{p}$ Kane model were performed, which are in very good agree-

ment with experiment. It has been shown that the heavy-hole character of the $H1$ conduction subband determines the electron-density distribution in the QW and enhances the Rashba spin splitting at large electron densities. These are unique properties of the first conduction subband of type III inverted heterostructures. An analytical model with $\beta k_{\parallel}^3$ dispersion has been employed to describe the spin splitting of the $H1$ conduction subband at small values of the in-plane wave-vector $k_{\parallel}$, rather than the $\alpha k_{\parallel}$ model commonly used for type I QW's. In addition, the relative magnitude of Rashba spin splitting in the $H1$ and $E2$ subbands has also been shown to be a consequence of the heavy hole character of the $H1$ subband and the light particle nature of the $E2$ subband, which is an admixture of the light hole and electron states.

ACKNOWLEDGMENTS

One of the authors, X. C. Zhang would like to express his thanks to the Volkswagen Stiftung for financial support. The authors would like to thank R. Winkler, Universität Erlangen, for many helpful discussions. The interest of J. Chu, Shanghai Institute of Technical Physics, CAS, is also appreciated. In addition, the support of the Deutsche Forschungsgemeinschaft, SFB 410, is gratefully acknowledged.

*Email: xczh@physik.uni-wuerzburg.de
On leave from Shanghai Institute of Technical Physics, Chinese Academy of Sciences, 200083 Shanghai, China.

[1] S. Datta and B. Das, Appl. Phys. Lett. **56**, 665 (1990).
[2] G. Dresselhaus, Phys. Rev. **100**, 580 (1955).
[3] E. I. Rashba, Fiz. Tverd. Tela (Leningrad) **2**, 1224 (1960) [Sov. Phys. Solid State **2**, 1109 (1960)].
[4] Y. A. Bychkov and E. I. Rashba, J. Phys. C **17**, 6039 (1984).
[5] H. L. Störmer, Z. Schlesinger, A. Chang, D. C. Tsui, A. C. Gossard, and W. Wiegmann, Phys. Rev. Lett. **51**, 126 (1983).
[6] U. Rössler, F. Malcher, and G. Lommer, in *Springer Series in Solid-State Sciences*, edited by G. Landwehr (Springer-Verlag, Berlin, Heidelberg, 1989), Vol. 87, p. 376.
[7] M. H. Weiler, in *Semiconductors and Semimetals*, edited by R. Willardson and A. C. Beer (Academic Press, New York, 1981), Vol. 16, p. 119.
[8] B. Das, S. Datta, and R. Reifenberger, Phys. Rev. B **41**, 8278 (1990).
[9] J. Nitta, T. Akazaki, H. Takayanagi, and T. Enoki, Phys. Rev. Lett. **78**, 1335 (1997).
[10] G. Engels, J. Lange, Th. Schäpers, and H. Lüth, Phys. Rev. B **55**, R1958 (1997).
[11] C. M. Hu, J. Nitta, T. Akazaki, H. Takayamgi, J. Osaka, P. Pfeffer, and W. Zawadzki, Phys. Rev. B **60**, 7736 (1999).
[12] F. J. Ohkawa and Y. Uemura, J. Phys. Soc. Jpn. **37**, 1325 (1974).
[13] A. Därr, J. P. Kotthaus, and T. Ando, in *Proceedings of the 13th International Conference on the Physics of Semiconductors*, edited by F. G. Fumi (North-Holland, Amsterdam, 1976), p. 774.
[14] R. Lassnig, Phys. Rev. B **31**, 8076 (1985).
[15] R. Winkler and U. Rössler, Phys. Rev. B **48**, 8918 (1993).
[16] E. A. de Andrada e Silva, G. C. la Rocca, and F. Bassani, Phys. Rev. B **55**, 16 293 (1997).
[17] P. Pfeffer and W. Zawadzki, Phys. Rev. B **59**, R5312 (1999).
[18] D. Grundler, Phys. Rev. Lett. **84**, 6074 (2000).
[19] R. Wollrab, R. Sizmann, F. Koch, J. Ziegler, and H. Maier, Semicond. Sci. Technol. **4**, 491 (1989).
[20] M. Schultz, F. Heinrichs, U. Merkt, T. Colin, T. Skauli, and S. Løvold, Semicond. Sci. Technol. **11**, 1168 (1996).
[21] F. Goschenhofer, J. Gerschütz, A. Pfeuffer-Jeschke, R. Hellmig, C. R. Becker, and G. Landwehr, J. Electron. Mater. **27**, 532 (1998).
[22] G. Landwehr, J. Gerschütz, S. Oehling, A. Pfeuffer-Jeschke, V. Latussek, and C. R. Becker, in *Proceedings of the 13th International Conference on the Electronic Properties of Two-Dimensional Systems* [Physica E (Amsterdam) **6**, 713 (2000)].
[23] N. F. Johnson, P. M. Hui, and H. Ehrenreich, Phys. Rev. Lett. **61**, 1993 (1988).
[24] Y. R. Lin-Liu and L. J. Sham, Phys. Rev. B **32**, 5561 (1985).
[25] M. Schultz, U. Merkt, A. Sonntag, U. Rössler, R. Winkler, T. Colin, P. Helgesen, T. Skauli, and S. Løvold, Phys. Rev. B **57**, 14 772 (1998).
[26] M. von Truchsess, V. Latussek, F. Goschenhofer, C. R. Becker, G. Landwehr, E. Batke, R. Sizmann, and P. Helgesen, Phys. Rev. B **51**, 17 618 (1995).
[27] C. R. Becker, V. Latussek, A. Pfeuffer-Jeschke, G. Landwehr, and L. W. Molenkamp, Phys. Rev. B **62**, 10 353 (2000).
[28] A. Pfeuffer-Jeschke, Ph.D. thesis, Universität Würzburg, Germany, 2000.
[29] C. K. Shih and W. E. Spicer, Phys. Rev. Lett. **58**, 2594 (1987).
[30] J. P. Laurenti, J. Camassel, A. Bouhemadou, B. Toulouse, R. Legros, and A. Lusson, J. Appl. Phys. **67**, 6454 (1990).
[31] This spin splitting is designated as *chiral* splitting, see reference in Ref. 32.
[32] R. Winkler, Phys. Rev. B **62**, 4245 (2000).
[33] R. Winkler, S. J. Papadakis, E. P. De Poortere, and M. Shayegan, Phys. Rev. Lett. **84**, 713 (1999), and references therein.
[34] M. J. Kane, N. Apsley, D. A. Anderson, L. L. Taylor, and T. Kerr, J. Phys. C **18**, 5629 (1985).
[35] G. Landwehr, Physica B (to be published).
[36] P. Pfeffer and W. Zawadzki, Phys. Rev. B **52**, R14 332 (1995).
[37] Here, β has been employed instead of the $\langle \beta_1 E_z \rangle$ term in Eqs. (10a) and (10b) of Ref. 32.